An affordable option to Au single crystals through cathodic corrosion of a wire: Fabrication, electrochemical behavior, and applications in electrocatalysis and spectroscopy

Mohamed M. Elnagar, Johannes M. Hermann, Timo Jacob, Ludwig. A. Kibler*

Institute of Electrochemistry, Ulm University, Albert-Einstein-Allee 47, 89081 Ulm, Germany
*Corresponding author: E-mail: ludwig.kibler@uni-ulm.de

ABSTRACT

Faceting and nanostructuring of polycrystalline gold electrodes by cathodic corrosion in concentrated potassium hydroxide electrolytes has been systematically studied at different electrode potentials. Current-potential curves for the restructured Au electrodes in 0.1 M H_2SO_4 show characteristic features of Au(111) facets in the double-layer and oxidation region. Thus, the modified Au electrodes adopt properties typically known for well-defined single crystal surfaces. Besides the preferential surface faceting, the electrochemically active surface area (EASA) is enhanced as a function of potential, concentration and time. Scanning electron micrographs show the formation of well-defined triangular pits and nanostructures with a specific orientation confirming the formation of (111)-facets. In this way, the behavior of single crystals is accompanied with the properties of nanoparticles which are of utmost interest in electrocatalysis and surface enhanced Raman spectroscopy (SERS). The electrocatalytic activity of the newly formed "Au(111)" surface from an Au wire has been tested towards the hydrogen evolution reaction (HER) and for the formic acid oxidation reaction (FAOR). The study of electrocatalytic reactions at these nanostructured electrodes allows to identify active centers, which are absent for extended single crystal surfaces. Adsorbed pyridine on the nanostructured Au electrodes directly shows SERS activity, while untreated polycrystalline Au is SERS-inactive. The use of cathodic corrosion of simple wires is a paradigm of SERS-applications in electrochemistry with clean Au electrodes that provide properties of Au(111) single crystals.

Keywords: Cathodic corrosion; Au(111); Nanostructuring; Formic acid oxidation reaction; Hydrogen evolution reaction; Surface-enhanced Raman Spectroscopy.

1. Introduction

The use of clean and structurally defined electrodes is well-established in many fields of interfacial electrochemistry, such as electrocatalysis, electroanalytics, bioelectrochemistry, energy conversion and storage, spectroelectrochemistry, corrosion, and material science [1,2]. In this way, structure-property relationships are obtained by studies of low-index and vicinal single crystals, shape- and size-controlled nanoparticles, poly-oriented spherical beads, or preferentially facetted electrode surfaces, etc. [3-6].

In contrast to simple electron transfer reactions, electrocatalytic reactions involve at least one adsorption step. For this reason, electrode kinetics is greatly influenced by adsorption energies of intermediates and often also by adsorbed electrolyte components, which in many cases are extremely sensitive to the local atomistic structure. Thus, the arrangement of surface atoms at the metal electrode may have a profound effect on the energetic pathways from reactants to products and, accordingly, the reaction rate, activity and selectivity [3,7,8].

In this regard, noble metal electrode surfaces have frequently been used in electrochemistry, because they are relatively easy to prepare and show very high stability for fundamental investigations. For a variety of reactions relevant for fundamental and applied research, the electrochemical behavior depends strongly on the crystallographic orientation, the mode of application (bulk vs. nanoparticles-based electrodes), as well as on the nature of the adsorbed species and the composition of the electrolyte. Therefore, noble metal electrodes play a major role in understanding structure-activity relationships [9-13].

Despite the valuable insights that can be obtained about the influence of extended surfaces of different structures on electrocatalytic activity and the electrochemical behavior, research with single-crystals is not possible in all laboratories. Such investigations are not only time-consuming and expensive, each electrode needs to be accurately fabricated, characterized, and handled to assure cleanliness and well-defined structure. Unfortunately, the effect of low-coordination sites that sometimes play a predominant role in electrocatalysis of nanoparticles cannot easily be studied with flat or stepped single crystal surfaces. In addition, the limited stability, which is apparent by electrodissolution or by irreversible structural deterioration under harsh conditions, restricts the utilization of costly single crystal electrodes and the reproducibility of data in certain electrochemical processes.

For these reasons, there are substantial research efforts in understanding the electrochemical behavior of well-defined nanostructured electrodes, bulk electrodes (for example

polyoriented bead single crystals) and electrodeposited nanostructures to substitute single crystal electrodes [3,11,14-18]. Au is considered the paradigm of stable electrode materials, because it is the only metal that is more stable than its oxides under standard conditions [19]. There is a variety of Au model systems, which are used in exchange to single crystals. These include thin Au films or Au nanoparticles on substrates such as glass or inert electrodes, faceted and nanostructured Au wires, nanoporous Au, *e.g.* obtained by dealloying of AgAu alloys and electrochemically treated Au samples [20-27]. In comparison, electrochemical faceting and nanostructuring of bulk wires afford clean and simple alternatives to substrate-based metal nanostructures prepared by first synthesizing colloidal nanostructures and then dispersing them onto the substrate surface. While the anodic treatment has long been used to clean polycrystalline Au, the cathodic treatment has retrieved interest on a fundamental and on a technological level [28-32].

Cathodic corrosion is an electrochemical etching process that induces substantial changes in the metal surfaces characterized by creating nanoparticles and a variety of etching features [33,34]. Recent studies hypothesized that cathodic corrosion occurs through the formation of metastable anionic species that are stabilized by non-reducible electrolyte cations [34-36]. The nature of these anionic species might be intermediate ternary metal hydrides, as suggested by theoretical DFT calculations that reveal the significant role of adsorbed hydrogen. Moreover, the presence of non-reducible cations, mostly alkali metal cations, is crucial for the cathodic corrosion process [35,36]. Previous theoretical studies demonstrate that alkali metal cations can specifically adsorb to metal electrode surfaces at low overpotentials in the hydrogen evolution region [37]. Furthermore, the experimental investigations indicate that the final surface structure and the etching features of the cathodically treated electrodes strongly depend on the nature and concentration of the adsorbed cations as well as the properties of the metal itself [35,38]. Hence, cathodic corrosion can be used as a powerful technique to tailor the structure of metal surfaces.

This study deals with the faceting and restructuring of polycrystalline Au wires in highly concentrated potassium hydroxide (KOH) electrolytes through cathodic corrosion. The effects of electrolyte concentrations and applied potentials on the structural changes, facet distribution, and roughening of Au surfaces have been studied in a systematic way using cyclic voltammetry (CV) and scanning electron microscopy (SEM). The electrochemical behavior of Au electrode surfaces in 0.1 M H_2SO_4 electrolyte is correlated to their local structure analyzed

by SEM before and after corrosion. In comparison to the recent studies of cathodic corrosion [35], this contribution presents new findings as a function of the applied parameters for the nanostructuring of Au surfaces. Cathodic corrosion of Au generates a single-crystal-like electrochemical behavior involving typical features of Au(111) electrodes. Therefore, the electrocatalytic behavior of this new type of nanostructured electrodes was investigated towards the hydrogen evolution reaction (HER) and for the formic acid oxidation reaction (FAOR) to identify reactive centers, which go beyond those of extended Au single crystal surfaces. Surface-enhanced Raman scattering (SERS) from well-defined surfaces would be superior to replace the randomly roughened electrode surfaces for in-situ monitoring of electrochemical and electrocatalytic reactions. For this reason, the Raman activity of adsorbed pyridine on the nanostructured Au electrodes with preferentially -oriented surfaces was studied with SERS.

2. Experimental

Electrode preparation. The polycrystalline gold electrodes (Au) were cut from a commercial wire (MaTecK, Jülich, Germany, 99.995%, Ø = 0.25 mm) with a wire cutter to 3 cm and thoroughly rinsed with ultra-pure water. Then, gold electrodes were cleaned by electropolishing in 0.1 M H_2SO_4 electrolyte at 10 V for 10 s at 20 ^oC and subsequent dissolution of the thin surface oxide layer in 1 M HCl. The electrodes were again thoroughly rinsed with ultra-pure water and flame-annealed before checking for their cleanliness by cyclic voltammetry in 0.1 M H_2SO_4. The electropolishing step was repeated until obtaining a clean and reproducible surface.

Electrochemical Measurements. Ultra-pure water (18.2 MΩ cm, TOC ≤ 3 ppb) was used for electrolyte preparation and apparatus cleaning. The solutions were made of H_2SO_4 (Merck, suprapur), $HClO_4$ (Sigma-Aldrich, trace metal basis), HCOOH (Merck, suprapur), and pyridine (≥99,9%, Sigma-Aldrich). The chemicals were used as obtained without further purification. The electrolytes were deaerated with nitrogen, before and during the experiments. All measurements in this study were carried out at room temperature (20 °C).

Cathodic polarization of Au electrodes. After measuring the voltammogram in 0.1 M H_2SO_4, the electrode was thoroughly rinsed with ultra-pure water to remove sulphate and then

transferred to a polypropylene cell, which was designed for the cathodic corrosion experiments. This cell comprises an aqueous solution of KOH (Sigma-Aldrich, 99.99%), a HydroFlex RHE electrode (Gaskatel), and titanium coil (MaTecK, Jülich, Germany, 99.7%) as a working electrolyte, a reference electrode, and a counter electrode, respectively. Following the immersion of the wire (2 mm length) in a defined electrolyte concentration, a constant negative potential was applied for 60 s. After that, the working electrode was removed, rinsed with ultra-pure, and transferred to the characterization cell, where it was contacted at −0.6 V vs. MSE.

Before SEM imaging, the electrode was rinsed, flame-annealed and characterized in 0.1 M H_2SO_4 to ensure the cleanliness of the electrode surface. Then, the electrode was rinsed with ultra-pure water and transferred to the polypropylene cell. After the cathodic polarization, the electrode was removed, rinsed with ultra-pure water, and stored for SEM characterization.

Characterization. A HEKA PG510 potentiostat was employed for all electrochemical experiments. A conventional three-electrode glass cell was utilized for the characterization of the electrodes in 0.1 M H_2SO_4 electrolyte using a saturated mercury/mercurous sulfate electrode (MSE) as a reference electrode and graphite rod as a counter electrode. The morphological characterization of the wires was examined by using a ZEISS LEO 1550 VP scanning electron microscope (SEM) operating at an acceleration voltage of 10 kV.

Raman Spectroscopy. Raman spectra were recorded with a Renishaw inVia confocal Raman-dual-laser system equipped with a Leica DM 2500 microscope. Spectra were obtained with a 633 nm laser at a power of 1.7 mW and an acquisition time of 20 s.

3. Results and discussion

The progression of surface faceting and nanostructuring of an Au wire induced by cathodic corrosion has been studied using cyclic voltammetry and scanning electron microscopy.

3.1. Cathodic corrosion process

The mechanism of cathodic corrosion is quite complex. The surface structure of the corroded electrodes depends on a variety of experimental parameters. From a fundamental point of view, the stability of Au electrode surfaces in contact with an electrolyte is strongly dependent on the applied potential. The surface tension shows a maximum at the potential of zero charge (pzc) where the surface has no excess charge. Lowering the electrode potential relative to the pzc induces a large surface stress [39]. At the same time, the bond strength between Au surface atoms is increased. More and more non-reducible cations are adsorbed at the negatively charged surface. Both the surface stress and the adsorbate induce substantial changes in surface structure by the rearrangement of atoms in order to increase the surface area and thus minimize surface charge density.

Here, gold surfaces were polarized at various negative potentials versus an internal reversible hydrogen electrode (RHE) for 60 s in a 10 M KOH electrolyte. The process of cathodic corrosion is challenging to study *operando* due to the harsh conditions, including high pH, strong evolution of hydrogen gas, and large electric current.

Cyclic voltammetry is used as a simple technique that gives valuable information about the entire electrode surface. In this regard, the cyclic voltammogram of gold surfaces in aqueous H_2SO_4 is very sensitive towards the orientation of the atoms on the electrode surface [40,41]. Therefore, to determine the initial stages of cathodic corrosion, the voltammograms of the gold electrodes before and after cathodic polarization were recorded in 0.1 M aqueous H_2SO_4 at a scan rate of s = 50 mV s^{-1}. In particular, the voltammetric profiles of the so-called double-layer and surface oxide regions show distinctive features which are attributed to distinct surface structures. As shown in Figure 1a, the anodic current peaks positive of 0.6 V vs. MSE at 0.90 V, 0.70 V, and 0.67 V are corresponding to surface oxidation of Au(111), Au(110), and (100)-oriented domains, respectively. The relative current or charge density of these anodic peaks directly reflects the distribution of the facets present on the surface of gold electrodes. There were no noticeable changes in the typical electrochemical behavior of polycrystalline Au electrodes in 10 M KOH as a function of potential after polarization at potentials between

0 and -0.5 V vs. RHE. Changes in the voltammetric behavior become visible in the double-layer and surface oxide regions after polarization at -0.5 and -0.6 V vs. RHE (Figures 1b and 1c). The current-potential curves display a development in the anodic peak around -0.12 V vs. MSE, which is attributed to the lifting the (111) surface reconstruction by specific adsorption of sulfate anions [40]. In addition, the enhancement in the surface oxidation peak at 0.9 V vs. MSE indicates an increase of (111) sites. Hence, these changes are considered as to the initial stages of cathodic corrosion. It will be seen that more pronounced structural changes appear together with an enhancement in the electrochemically active surface area (EASA) after lowering the electrode potential to -0.8 V. The cathodic corrosion process of Au surfaces starts at a potential negative of the equilibrium potential of the hydrogen evolution reaction. Theoretical calculations reveal the crucial role of adsorbed hydrogen (H_{ads}) in cathodic corrosion through investigating the effect of H_{ads} on the potential-dependent surface energy. The results show an energetic driving force for the creation of surface area at potentials where the cathodic corrosion starts experimentally [35]. Thus, the role of adsorbed hydrogen should be considered. At a certain point, the H coverage might dramatically increase and facilitate surface mobility [42].

The electrochemical characterizations reveal changes in the surface structure after cathodic polarization. Consequently, monitoring the surface morphology provides more insight into the cathodic corrosion of Au surfaces. Therefore, ex-situ SEM was utilized for the structural characterization of the cathodically corroded Au wires. The micrographs are illustrated in Figures 1d and 1e. There are no obvious signs of corrosion on the wires polarized at potentials positive of -0.7 V vs. RHE. Apparently, the SEM resolution is not sufficient to monitor very slight structural changes at the Au surface. As the applied potential is lowered to -0.8 V vs. RHE, the formation of etching pits is detectable, however, only at the tip of the corroded Au wire, as shown in Figure 1e compared to the as-polished surface in Figure 1d. It is worth mentioning that the polarization at this potential increases noticeably the surface area as indicated from the cyclic voltammograms, so the study of these surfaces is possible with SEM.

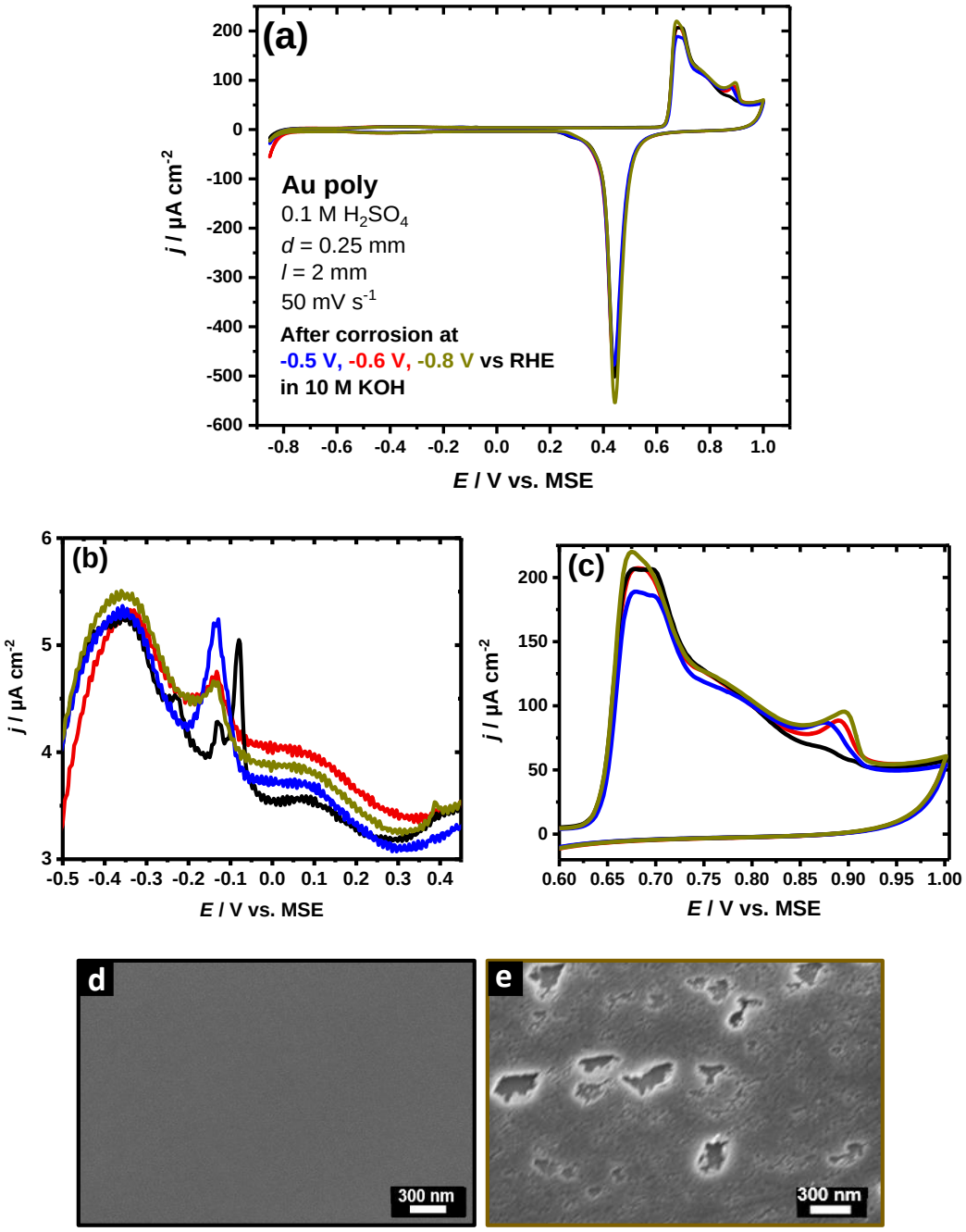

Figure 1: (a) Cyclic voltammograms of an Au wire in 0.1 M H_2SO_4 at a scan rate of 50 mV s^{-1} before and after negative polarization in 10 M KOH at -0.5, -0.6 and -0.8 V vs. RHE for 60 seconds. The current density is related to the geometric surface area. The double-layer region and voltammetric peaks for surface oxidation of (a) are magnified in (b) and (c), respectively. (d) SEM micrograph of the pristine Au surface. (e) Au surface after polarization at -0.8 V vs. RHE in 10 M KOH for 60 seconds.

3.2. Fabrication of Au surfaces with preferential (111)-texture

A prominent sign of cathodic corrosion of Au surfaces after polarization at negative potentials in 10 M KOH electrolyte is the alteration of facet distributions with an enhancement in the (111) domains. Consequently, the applied potential was further lowered to -3.5 V vs. RHE to evaluate the cathodic corrosion of Au surfaces in the same electrolyte for 60 s. Figures 2a and 2b display the voltammetric profiles for Au electrodes in 0.1 M aqueous H_2SO_4 at a scan rate of s = 50 mV s^{-1} before (black curves) and after cathodic polarization (red curves). The cyclic voltammetry profiles were recorded for the lower and upper potential limits of E_L = −0.85 and E_U = 1 V and for E_L =−0.85 and E_U = 0.6 V to monitor the changes in the orientation of surface facets. The current density was determined by dividing the measured current by the exposed geometrical electrode surface area (Figure 2a) or alternatively by considering the increase in EASA (Figure 2b). The scale of the current density for the double-layer region (E_L =−0.85 and E_U = 0.6 V vs. MSE) is enlarged by a factor of 30. Interestingly, the cathodically polarized electrode shows a single-crystal-like electrochemical behavior with characteristic features of Au(111) electrodes. This electrode with the highest (111) contribution is referred to as "Au(111)". The voltammograms in Figure 2 (red curves) reveal the following characteristic features in the double-layer and oxide regions: (i) an anodic peak at -0.12 V corresponding to the lifting of the Au(111) reconstruction by sulphate adsorption and a cathodic peak at -0.19 V corresponding to sulphate desorption; (ii) a sharp anodic spike at 0.38 V and a sharp cathodic spike at 0.35 V that are attributed to the well-known adlayer phase transition of adsorbed sulphate on Au(111); (iii) a sharp peak at 0.90 V assigned to surface oxide formation at Au(111)-facets; and (iv) an increase in the charge density of the reduction peak at 0.45 V after including the increase in EASA (Figure 2b) compared to pristine Au electrode (black curve). These features are electrochemical fingerprints unique to well-defined Au(111) electrode surfaces [40,43]. The charge densities of the surface oxidation peak at 0.90 V for the pristine Au electrode and after polarization at -3.5 V vs. RHE are 96 and 426 μC cm^{-2}, respectively. In agreement with this increase by a factor of 4.4, the surface area of the modified electrode is increased by a factor of 4.2 as indicated by the increase in the charge of the double-layer capacity.

Further indications of a larger surface area with distinct etching features monitored by SEM for the corroded wire at -3.5 vs. RHE are presented in Figures 2c-g. The SEM examination illustrates that the whole area of the wire in contact with the electrolyte is completely

corroded, however, with different local structures. As shown in the micrographs depicted in Figures 2d and 2e, cathodic corrosion generates a roughened surface accompanied by small preferentially-oriented nanoparticles at the tip-region of the wire as indicated in the high magnification image in Figure 2e. The size of these nanoparticles is in the range of 40 to 60 nm. The tip-region, which is entirely covered with nanoparticles is highlighted in green, as illustrated in Figure 2c. In addition to these nanoparticles, well-defined triangular pits with different size are detected at the rest of the corroded wire away from the tip-region (red-rimmed). Some of these triangular pits are highlighted in blue color. From a structure and symmetry point of view, the triangular pits are indicative of a (111)-surface [44]. The formation of the nanoparticles and the triangular pits induced by cathodic corrosion is indeed the reason for an appreciable increase in the electrode surface area as supported by the electrochemical characterization. After cathodic polarization of polycrystalline Au electrodes at a relatively high voltage of -3.5 V, the surface is supposed to become quite brittle (large surface stress) and partial decomposition (dissolution) appears to increase the surface to extenuate the constrain. The electrochemical characterization and the SEM analysis are complementing each other, both methods reveal the formation of Au(111)-oriented surfaces with high EASA after cathodic polarization. It should be emphasized that the (111)-facet is the most thermodynamically stable among all extended surfaces [45]. Furthermore, the formation of (111) facets is found to be driven by adsorption of K^+ cations.

Single-crystalline thin films of Au(111) can be prepared by epitaxial growth on scratch-free mica. However, these films are often not stable and delaminate after a few minutes in water [20]. Furthermore, ca. 200 nm thick Au films evaporated onto special glass, with a thin chromium undercoating to enhance adhesion, produce well-ordered (111) surfaces after annealing [21]. However, chromium can form alloys with Au (for example $AuCr_3$) which can behave chemically different to clean gold films [46]. Moreover, a highly ordered Au (111) phase can be prepared by vacuum deposition on a polycrystalline gold disk substrate at 300 °C followed by anneal-quenching treatment [22]. Another approach is the seed mediated growth of electrodeposited Au-nanoparticles onto a glassy carbon electrode from a solution of $H[AuCl_4]$ + NH_2OH at pH 0.5, resulting in Au(111) facets [23]. In comparison, nanostructuring and faceting of an Au wire to fabricate Au surfaces with preferential (111)-texture through cathodic corrosion is more affordable. In addition, comparing the cyclic voltammogram profiles indicate that the sharpness of the surface oxidation peak of the (111)-

facets is higher for the electrodes fabricated through cathodic corrosion than those obtained by vacuum deposition or seed-mediated growth of electrodeposited gold-nanoparticles.

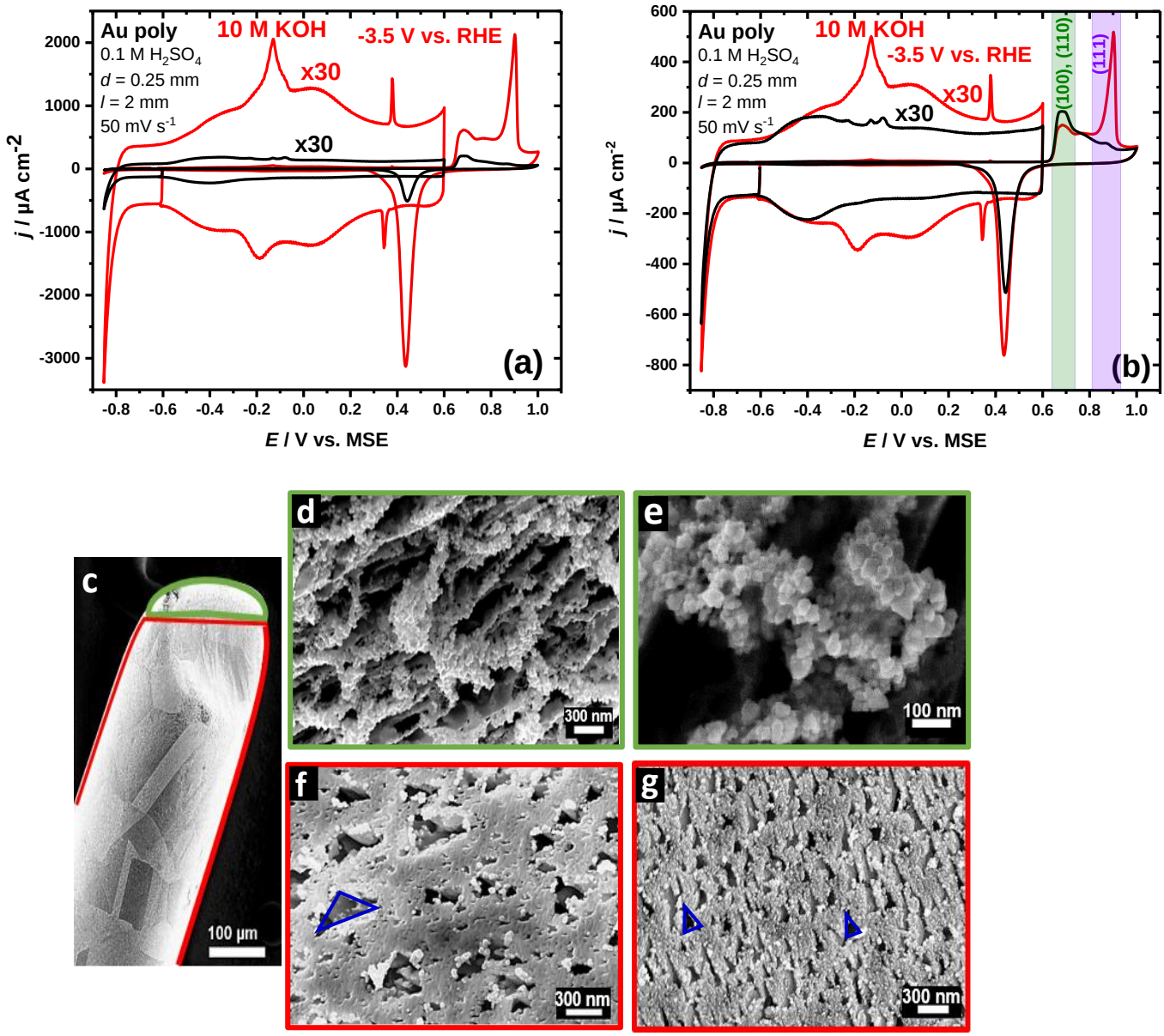

Figure 2: (a) Cyclic voltammograms for pristine polycrystalline gold in 0.1 M H_2SO_4 at a scan rate of 50 mV s^{-1} before (black curves) and after (red curves) polarization in 10 M KOH at -3.5 V vs. RHE for 60 seconds. The current density is related to the geometric surface area. The scale of the current density for the double-layer region is enlarged by a factor of 30. (b) The same date as in (a) with the current normalized to the electrochemically active surface area. (c-g) SEM images of an Au wire after polarization in 10 M KOH at –3.5 V vs. RHE for 60 seconds. SEM images of the tip-region (d,e – green-rimmed) are systematically different to those obtained away from the tip (f,g – red-rimmed).

3.3. Effect of electrolyte concentration and applied voltage

3.3.1. Electrochemical characterization

Since the final surface structure depends strongly on the applied conditions, the effect of the KOH concentration and applied negative voltages have been systematically investigated. From this perspective, Au wires were cathodically polarized at different voltages from -1 to -5.5 V vs. RHE in different concentrations of aqueous KOH electrolyte in the range of 2 – 20 M for 60 s. Polarization of Au wires in 2 M KOH electrolyte in this range of voltages for 60 s hardly influences the Au surface structure. In contrast, manifest changes in the facet distribution and the EASA have been detected by increasing the electrolyte concentration to 5 M and higher. High near-surface concentration of K^+ is supposed to be essential for cathodic corrosion because the highly negative potentials can only be achieved with appropriate counter-charges.

Figures 3a and 3b show changes in the first cycle of the current-potential curves for Au electrodes after corrosion in 5 M and 10 M KOH electrolytes compared to the untreated electrodes. The current in these voltammetry profiles is normalized to the EASA, not anymore to the geometric surface area. As observed in Figures 3a and 3b, the characteristic features of the surface structure are substantially altered as a function of the experimental conditions. These changeable features include (i) the shape and intensity of lifting of the surface reconstruction peak at 0.10 V; (ii) the sharpness and the charge density of the sulphate spike at 0.38 V; (iii) the intensity of surface oxidation peaks at positive of 0.60 V which corresponding to the facet preferences; and (iv) the charge density of the reduction peak at 0.45 V. It is clear that the sharpness of the sulphate spike and the intensity of the surface oxidation peak of the (111)-facet are correlated to each other. Furthermore, these peaks serve as sensitive indicators of the surface structure. For a clear overview, the increase in EASA and changes in facet distribution as a function of the electrolyte concentrations and the applied voltages were analyzed by cyclic voltammograms. EASA factors have been determined by comparing the double-layer capacity of the corroded and the untreated electrodes at -0.60 V vs. MSE. Moreover, the ratio between facets is obtained by dividing the current density of (111)-facet peak at -0.90 V vs. MSE by the current density of (110)-facet peak at 0.70 V vs. MSE in the oxidation region. These values give the same trends obtained by dividing the charge density of the (111)- facet peak by the charge density of (100) and (110)- facets in the oxidation region.

An overview of EASA factors and the facet distributions is shown in Figures 3c and 3d. After polarizing the wires at -1.5 V $\leq E \leq$ -1 V vs. RHE, there is no clear difference in the EASA factor and facet distribution values as a function of KOH concentration. However, at more negative potentials $\leq$ -1.5 V vs. RHE, the concentration of K^+ cations strongly affects the EASA and the orientation of the surface.

Recently, the cathodic corrosion behavior of Au wire has been investigated after treatment in 5 M KOH [35]. It was observed that the polarization of Au wire KOH electrolyte at -3 V vs. RHE induces the formation of disordered surface lacking well-defined oxide features in the first cycle. Furthermore, there are any characteristic features detected in the double-layer region. In contrast, we find that the EASA and the ratio of (111)-facets are increased after polarization in 5 M KOH, especially at highly negative potentials. Furthermore, it is obvious from the voltammograms in Figure 3a that there are significant features arise in the double-layer region upon polarization at different voltages, which corresponding to a well-defined surface. Exploiting the conditions for cathodic corrosion of Au surfaces leads to the formation of novel nanostructured and faceted electrodes with exceptional features as a function of KOH concentration and the applied voltage.

Further increase of KOH concentration up to 10 M induces considerable changes identified by a distinguished enhancement in EASA and in the ratio of the (111)-facet compared to 15 M and 20 M, particularly at negative potentials lower than -2.5 V. Furthermore, the maximal contribution of (111)-facets is shifted to less negative potentials for concentrations of 15 M and 20 M (Inset in Figure 3d). The observed trends for these highly concentrated, almost saturated KOH electrolytes (15–20 M) might be due to the low concentration of free water needed for the hydrogen evolution reaction. Therefore, cathodic polarization under these conditions is accompanied by less hydrogen evolution that is a driving force for cathodic corrosion. Moreover, the mean activity coefficient of concentrated KOH solutions (> 10 M) is larger than 1 [47], which implies that the ions experience strong repelling forces.

Figure 3c shows that the increase in EASA is greatly enhancing with applying more negative potentials for KOH concentration between 5 and 20 M. The maximum EASA factor is approximately 6 after polarization of the Au wires at -5 V vs. RHE in 10 M KOH (inset in Figure 3c). Additionally, the sharp features of (111)-surface are significantly enhanced by polarizing the Au electrodes at more negative potentials until a certain KOH concentration before they decrease at more concentrated solution (Figure 3d). The maximum ratio of (111)-facets

compared to other facets is 3.5 after the corrosion of Au electrodes at -3.5 V vs. RHE in 10 M KOH. These trends as a function of the applied voltage can be explained in the light of the vigorous hydrogen evolution at more negative voltages. The coverage of adsorbed hydrogen might dramatically increase leading to higher mobility of Au surface atoms, which facilitates restructuring of the surface [42]. Moreover, DFT calculations suggested that alkali metal cations can be specifically adsorbed onto fcc-transition metal surfaces at potentials below the potential range of hydrogen evolution in alkaline solutions [37]. So, specific adsorption with high coverage of K^+ is expected at higher negative voltages. After polarization at potentials more negative of -3.5V vs. RHE, the contribution of (111)-facets decreases gradually, possibly due to stronger Au dissolution and the formation of less ordered surfaces.

Due to the high current flow during the cathodic polarization of the Au wires, the *IR*-drop needs to be considered to determine the actual potentials. Electrochemical impedance spectroscopy measurements were performed in order to determine the resistance *R* of the KOH electrolytes. The *IR*-drop was calculated by multiplying the electrolyte resistance by the value of the current flow during the cathodic polarization. Figures 4a and 4b show the same data as Figure 3c and 3d after correction for the *IR*-drop. Similar trends as in Figure 3c and 3d are observed for the EASA factor and the facet distribution. Furthermore, it is obvious from the *IR*-corrected data that more negative potentials are achieved for increasing KOH concentration. These observations highlight the importance of the alkali metal cation in enabling the cathodic polarization of Au surfaces.

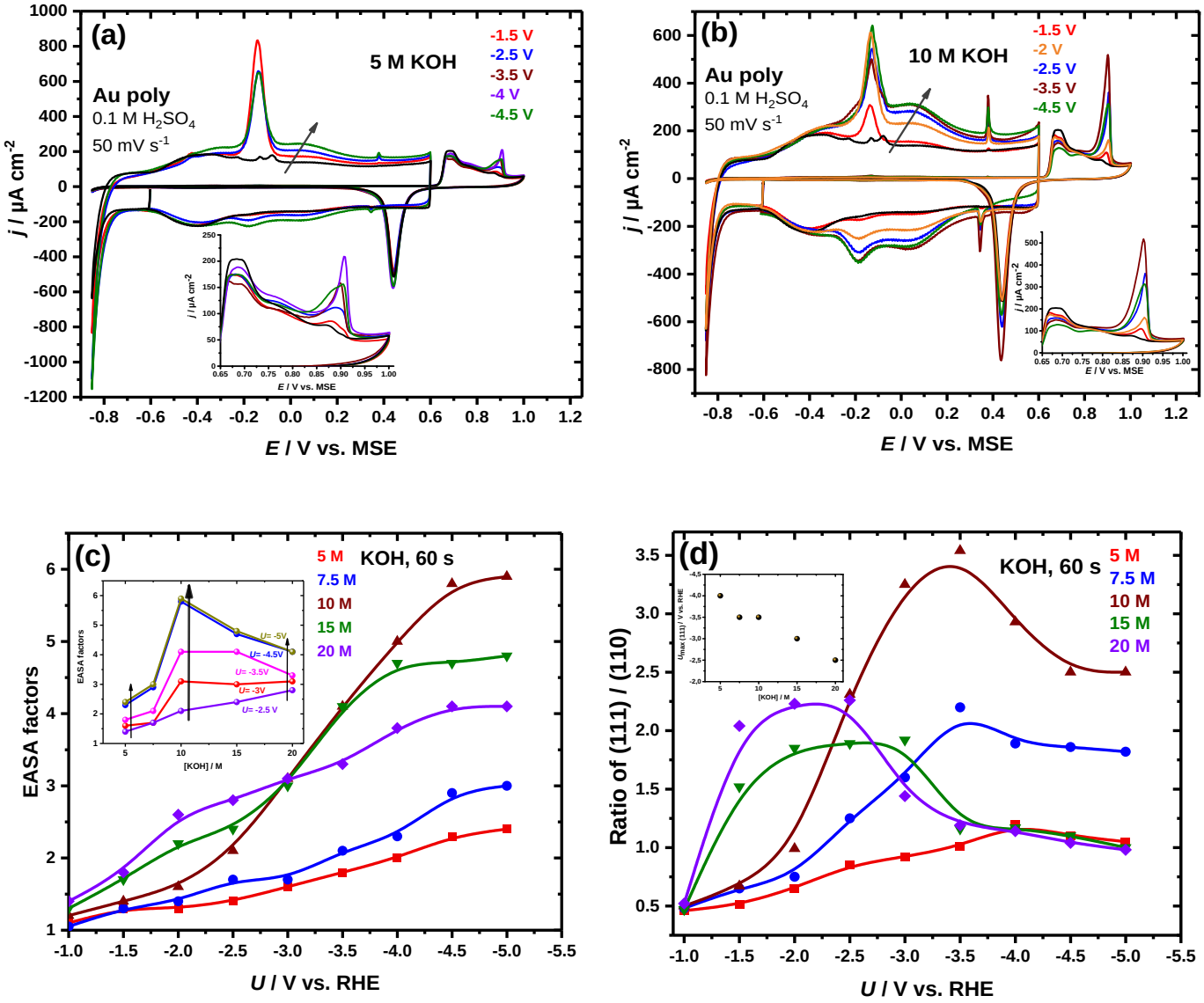

Figure 3: Cyclic voltammograms for gold in 0.1 M H_2SO_4 at a scan rate of 50 mV s^{-1} before and after polarization in (a) 5 M KOH and (b) 10 M KOH at different voltages vs. RHE for 60 seconds. The insets in (a) and (b) show a close-up of the oxidation region. The current scale of the double-layer region is enlarged 30 times. (c) EASA factor and (d) ratio of (111)/(110) surface facets after polarization of Au in KOH solutions of different concentration as a function of the voltage applied for 60 seconds.

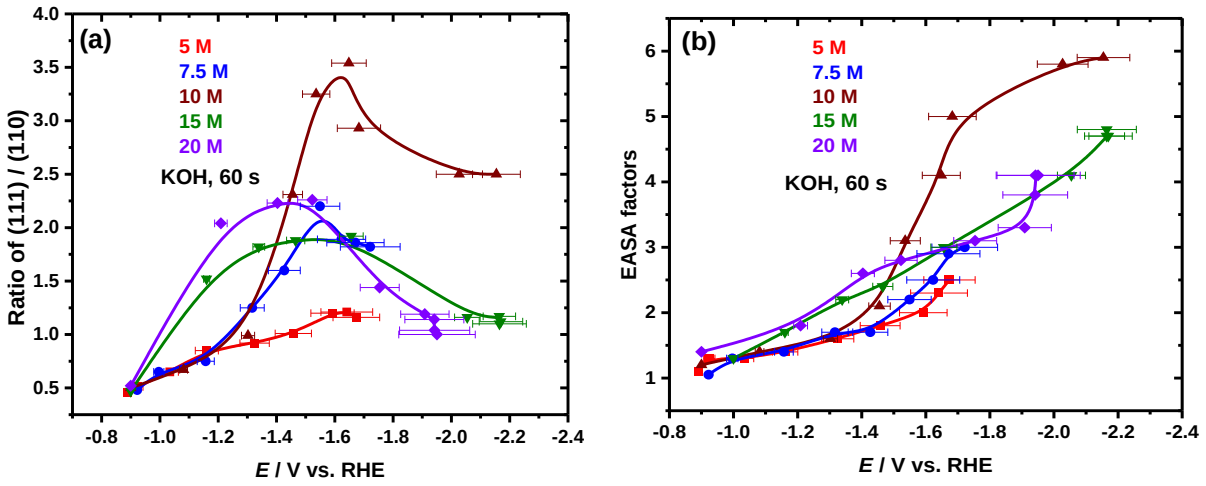

Figure 4: (a) and (b) are the same data as in Figures 3c and 3d after correction for the IR drop.

3.3.2. SEM analysis

We systematically investigated how the applied electrode potential and the KOH concentration impact the surface morphology in the cathodic corrosion process. Local structural changes induced for of Au surfaces in 10 M KOH after polarization at different potentials for 60 s are shown in Figure 5. A schematic illustrating different regions of the Au wire is shown at the top above the SEM images in Figure 5a-j. Cathodic corrosion starts at the tip of the Au wire and gradually spreads to the rest of the wire as a function of the applied voltage and time. For constant time of 1 min, the corroded length of the wire exposed by 2 mm to the electrolyte is larger at more negative potentials, complete corrosion is observed at -2 V vs. RHE (Figure 5k). Not only the corroded area increases at more negative potetial, also the extent of corrosion features is more severe. After polarization at -1.5 V vs. RHE, the Au tip is restructured showing a corrugated surface with step edges of 90˚, while triangular pits appear at a distance from the tip (Figures 5a and 5b). By lowering the applied potential to -2 V vs. RHE, the surface becomes rougher and small clusters of irregular nanoparticles appear at the tip. At the same time, the density of the triangular pits away from the tip is increased (Figures 5c and 5d). Further change of the applied potential to values negative of -2 V vs. RHE generates highly rough surfaces, again with nanoparticles at the tip and triangular pits away from the tip. While nanoparticles become denser and preferentially-oriented at the tip, they also start to cover the surface away from the tip. It seems that the process of cathodic corrosion locally proceeds via the same mechanism, albeit it is much faster at the tip of the

wire, where the electric field is much stronger. Moreover, the quantity of the well-defined triangular pits increases after polarization at voltages up to -3.5 V vs. RHE (Figures 5e, f). on the other hand, as can be seen in Figures 5g-j, the amount of such well-ordered triangular pits is substantially lower for electrodes polarized at -4 V and -5 V vs. RHE. Furthermore, the number of the nanoparticles significantly increases compared to that of triangular pits. These trends obtained from SEM analysis are consistent with the electrochemical behavior, as shown in Figure 3. The electrochemical characterization shows that the EASA increases with more negative corrosion potential (Figure 3c). Both the formation of nanoparticles and the partial dissolution of the surface help to increase the surface area. Moreover, the smaller contribution of (111)-facets after polarization at voltages negative of -3.5 V vs. RHE may be due to the decrease in the density of the well-defined triangular pits of (111)-texture.

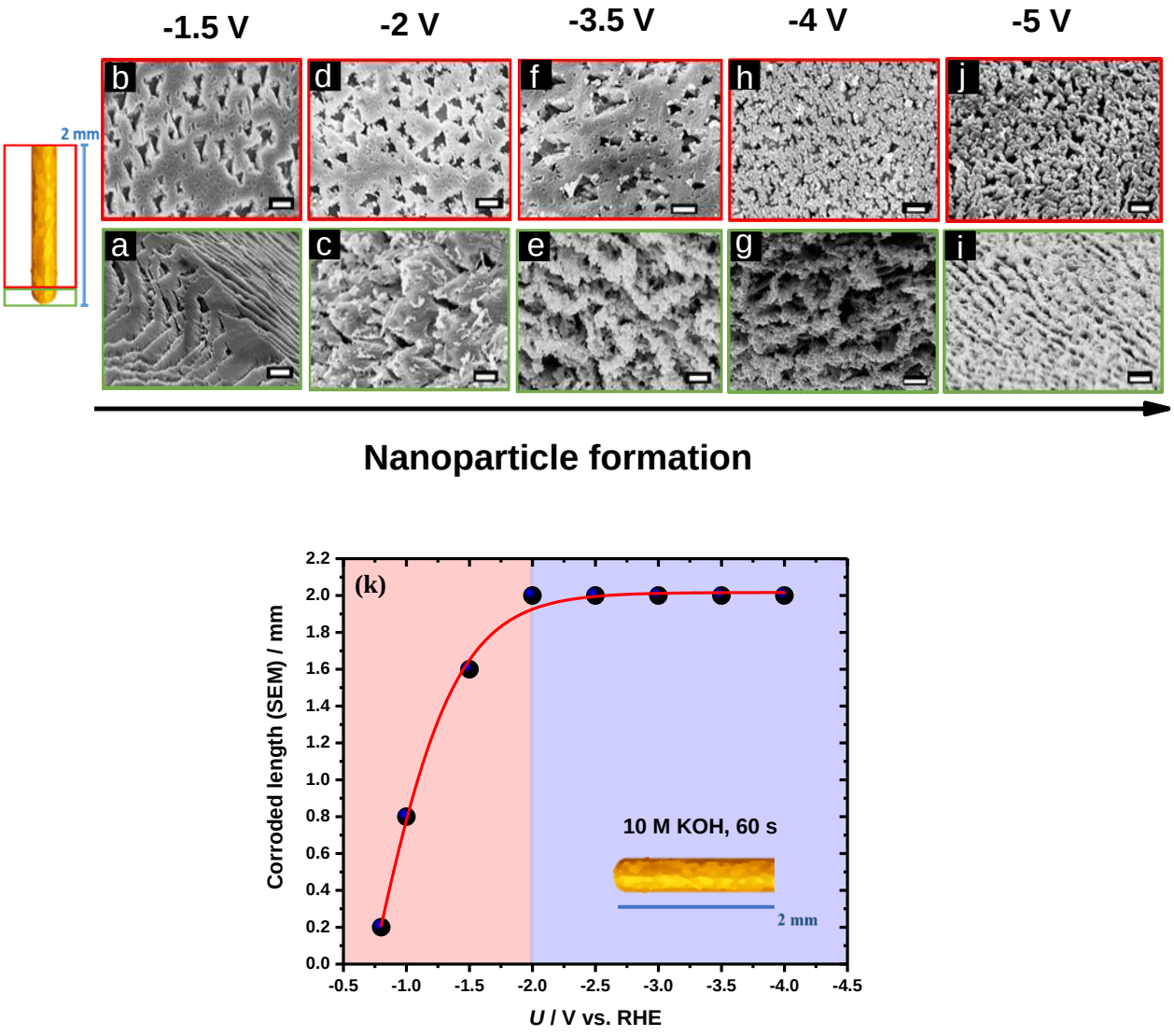

Figure 5: SEM micrographs of Au electrodes corroded in 10 M KOH for 60 s at (a, b) -1.5 V, (c, d) -2 V, (e, f) -3.5 V and (g, h) -4 V, (i, j) -5 V vs. RHE. The scale bar is 300 nm. (k) Corroded length of the Au wire electrode as a function of the applied potential. A schematic illustrating the local structure of the corroded wire is shown above the SEM micrographs.

To determine the effect of KOH concentration on local structural changes of the Au surfaces, we compare SEM images after polarization for 60 s in 5 M, 10 M, and 20 M of KOH at -1.5 V and -3 V vs. RHE. The corrosion features are more pronounced after treatment in 10 M KOH compared to 5 M and 20 M, as observed in Figure 6. Still, a similar trend as a function of the applied potential for the cathodically corroded electrodes in 10 M KOH is noticed compared to polarization in 5 M and 20 M. For example, small etching pits at the tip are detected for the polarized wire at -1.5 V vs. RHE in 5 M KOH (Figures 6a and 6b). The density of triangular pits increases further, the structure becomes relatively ordered after polarization at -3 V vs. RHE (Figures 6c and 6d), thus indicating higher EASA and the presence of (111)-facets. Comparing the corrosion behavior of Au induced by varying the concentration reveals the following features. The level of corrosion is more severe as well as the triangular pits are more well-defined and larger after polarization at -1.5 V (Figures 6e and 6f) or -3 V vs. RHE (Figures 6g and 6h) in 10 M compared to 5 M KOH (Figures 6a-d). Further increase of KOH concentrations to 20 M induces the formation of corrugated surfaces with more disordered pits (Figures 6i-l) but still more corroded than those obtained after polarization in 5 M. These results are complemented with the electrochemical data which show that polarization of Au in 10 M KOH at -3 V vs. RHE generates well-defined (111)-surfaces compared to the polarization in 5 M and 20 M electrolyte. These findings highlight that the SEM analysis and cyclic voltammetry results are complementing each other concerning the development of surface roughness and preferential faceting as a function of KOH concentration and applied potential.

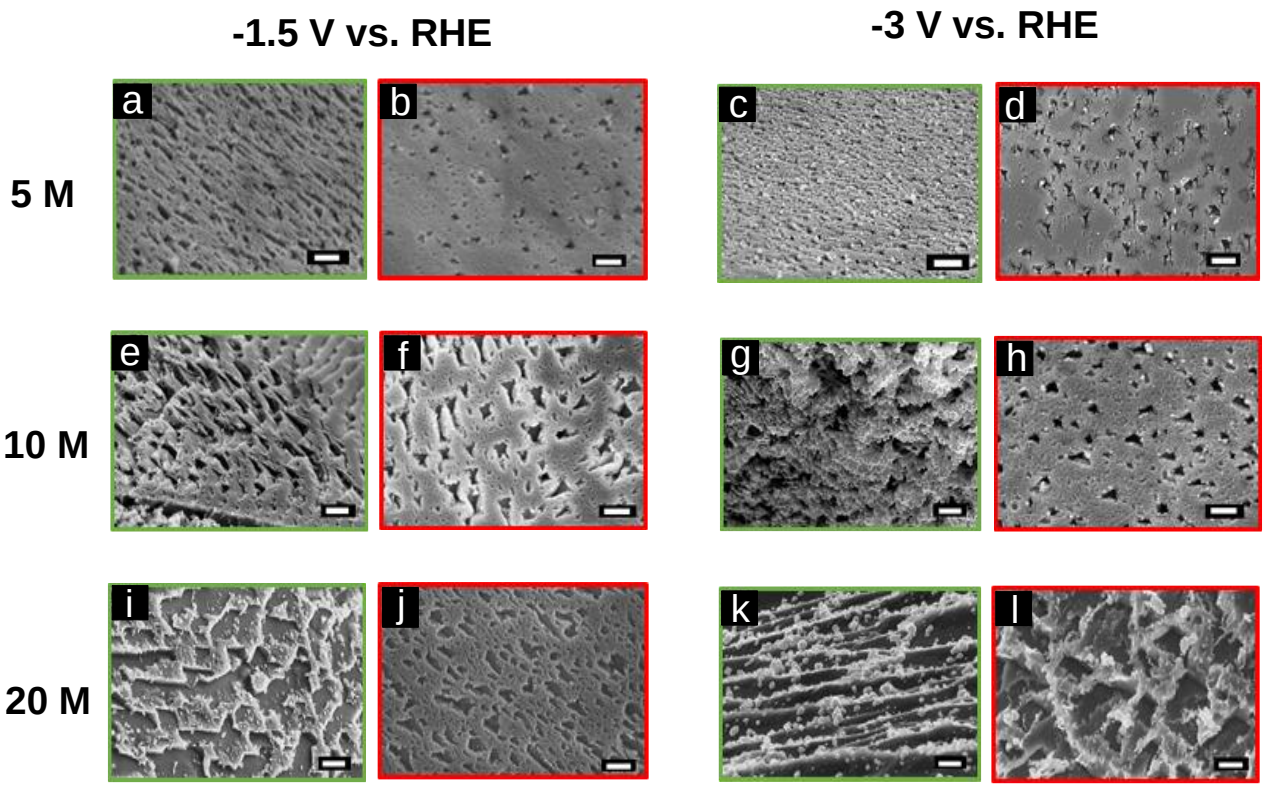

Figure 6: SEM micrographs of Au electrodes corroded in 5 M KOH for 60 s at (a, b) -1.5 V and (c, d) -3 V vs. RHE, 10 M KOH at (e, f) -1.5 V and (g, h) -3 V vs. RHE and 20 M KOH at (i, j) -1.5 V and (k, l) -3 V vs. RHE. Scale bare is 300 nm. SEM images of the tip-region (green-rimmed) are different to those obtained away from the tip (red-rimmed).

3.4. The electrocatalytic behavior of Au after cathodic corrosion

While tailoring surface properties is used to design new catalysts, the (electro)catalytic response of an electrode surface sheds light on its surface structure. This is especially true for so-called structure-sensitive reactions, which can inversely be used to study dynamics of structural changes [48]. From both of these fundamental points of view, the electrocatalytic behavior of the nanostructured electrodes obtained by cathodic corrosion has been investigated towards the formic acid oxidation reaction (FAOR) and the hydrogen evolution reaction (HER). We first examine the electrocatalytic activity of electrodes, which were polarized in 10 M KOH and characterized by a different extent of (111)-facets (see Figure 3d), and then compared those with the behavior of an Au(111) single-crystal. Figure 7a displays current-potential curves for the various Au electrodes in 0.1 M $HClO_4$ and 0.1 M HCOOH at a scan rate of s = 10 mV s^{-1} to study FAOR.

As can be seen in Figure 7b, the specific activity of the electrodes was obtained by normalizing to the EASA by using data from Figure 3d. The FAOR starts around -0.35 V vs. MSE for all Au electrodes under study. However, the formic acid oxidation current depends on the contribution of (111)-facets. The oxidation current is significantly enhanced as more and more (111)-facets are present. Furthermore, the bell-shaped curve of formic acid oxidation with a step-up in current corresponding to a phase transition within the strongly bound formate on (111) surface at 0.52 V is exceedingly pronounced for the (111)-nanostructured electrodes. Essentially, the sharpness of this step-up in the current (kink) for FAOR is correlated to the contribution of (111) facets [49]. The trend observed for this kink is in excellent agreement with the systematic series of sulfate spikes for Au in H_2SO_4 (Figure 3b). So far, this sudden change in the current for FAOR at 0.52 V has only been reported for large and well-ordered Au(111) single crystal surfaces [50,51]. This is a marked sign about the high-quality of the "Au(111)" electrodes through simple fabrication by cathodic corrosion.

The HER activity of the fabricated Au electrodes was tested in 0.1 M H_2SO_4 electrolyte solution at a scan rate of s = 1 mV s^{-1}. Slow negative scans are shown in Figure 7c to compare quasi-steady-state HER activities for the nanostructured Au surfaces with different (111)-contribution and the polycrystalline Au electrode. The HER onset potential for the polycrystalline gold is around -0.74 V vs. MSE, which is similar to the behavior of Au(111) single-crystals [42,52]. Remarkably, the HER onset potential is shifted to more positive

potentials (lower overpotential!) at around -0.66 V vs. MSE (0.05 V vs. RHE) for the nanostructured electrodes with a higher (111)-contribution. It is obvious that the nanostructured electrode with the maximum (111)-contribution “Au(111)” (blue curve) is more active for HER than Au(111), and even more active than other planar Au single crystal surfaces. Therefore, the role of low-coordination sites, the impact of nanostructures is considered [53]. Moreover, the differences to of FAOR activity is stunning: “Au(111)” and Au(111) show almost identical behavior. Low-coordination sites do not seem to be very active for FAOR, despite their enhanced HER activity. These electrocatalytic reactions are not only sensitive to structural changes, the importance of terraces, steps, and defect sites for the reaction mechanism can efficiently be identified. The reactive centers of maximum activity for HER and FAOR seem to be related to different atomic ensembles.

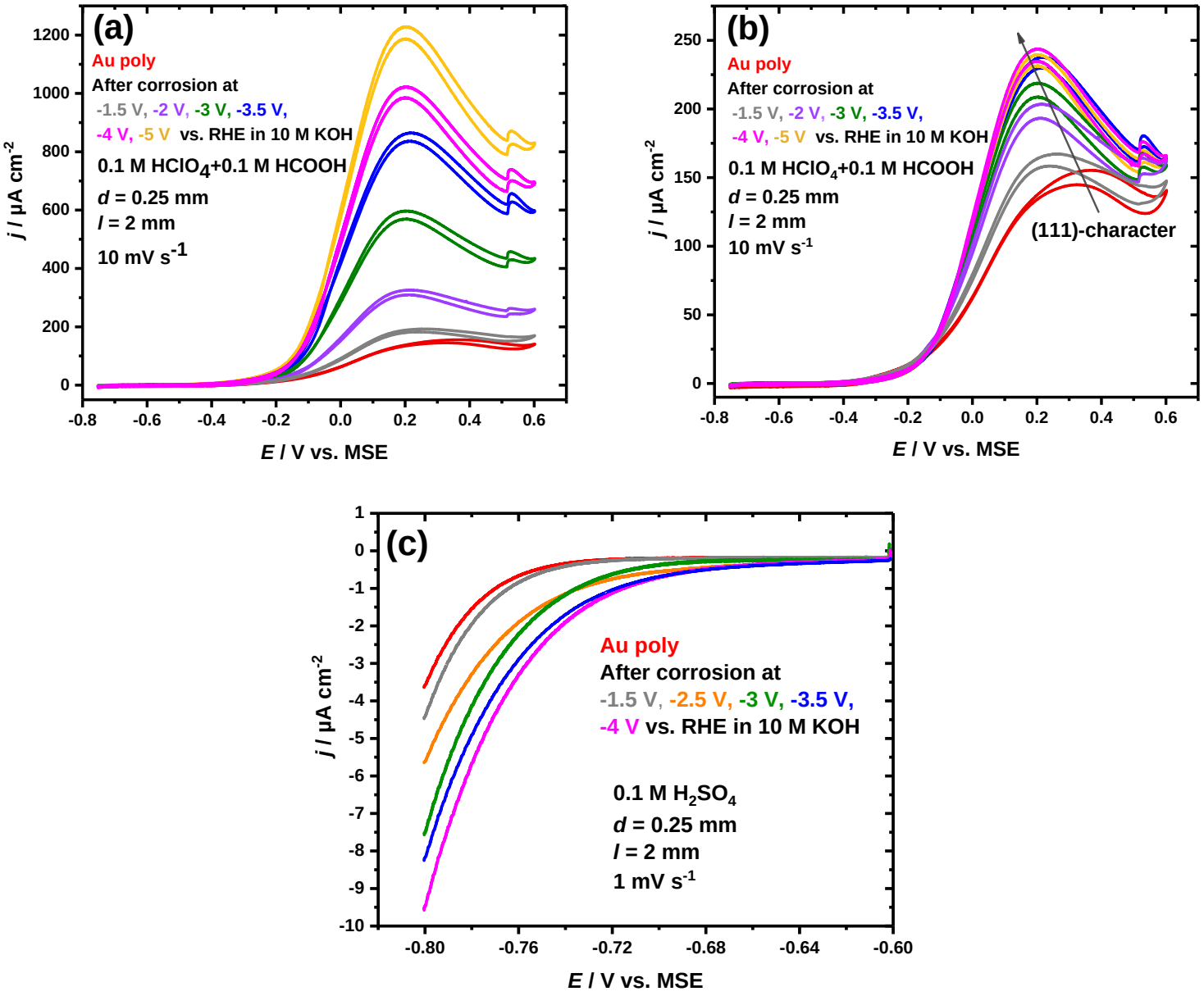

Figure 7: (a) Current-potential curves of polycrystalline gold in 0.1 M $HClO_4$ + 0.1 HCOOH at a scan rate of 10 mV s^{-1} before and after polarization in 10 M KOH at different voltages for 60 seconds leading to "Au(111)" quasi-single-crystal-behavior. (b) Same data as in (a) with current normalized to electrochemically active surface area. (c) Current-potential curves of polycrystalline gold in 0.1 M H_2SO_4 at a scan rate of 1 mV s^{-1} before and after polarization in 10 M KOH at different voltages for 60 seconds.

3.5. SERS-activity of the preferentially oriented electrodes

Pyridine is considered an ideal molecule for fundamental investigations of adsorption of neutral molecules at the electrified solid/liquid interface as well as for surface-enhanced Raman spectroscopy (SERS). It is therefore ideally suited to test new SERS substrates.

The electrochemical behavior of the Au electrodes in 0.1 M pyridine + 0.05 M $HClO_4$ at scan rate of s = 50 mV s^{-1} is shown in Figure 8a. The cyclic voltammogram for the polycrystalline Au electrode (black curve) shows an anodic peak at around -0.45 V vs. MSE corresponding to an orientational change of adsorbed pyridine, where the upright configuration is present. The peak potential depends on the pyridine concentration [54,55]. For the nanostructured electrodes, this peak is more pronounced at it appears together with a shoulder and a spike. An additional peak at around 0 V vs. MSE emerges for the nanostructured electrodes, which is related to another phase transition where the adsorption of a second layer of pyridine was suggested [14,19]. These peaks, which are characteristic features for Au(111) surface, are more marked for the Au electrodes with a higher (111)-contribution.

There is no Raman effect for smooth surfaces, because they do not provide surface plasmon resonance (SPR) [56]. Therefore, most of the studies have been restricted to randomly roughened substrates with ill-defined surfaces. Spectral analysis is then hampered which limits the practical applications of SERS. In this regard, shell-isolated nanoparticle-enhanced Raman spectroscopy (SHINERS) was developed, in which the Raman signal amplification is provided by gold nanoparticles covered by ultrathin SiO_2 or Al_2O_3 [57, 58]. Gold-core silica shell (Au@SiO_2) nanoparticles are used to enhance Raman signals from species on atomically flat single-crystal surfaces. Still, the fabrication of clean single-crystal surfaces decorated with SHINERS nanoparticles is quite difficult and involves multiple steps. Therefore, introducing simple methods for the preparation of clean SERS substrates with preferentially-oriented surfaces is extremely important and promising. The Raman activity of adsorbed pyridine on the nanostructured Au electrode with the maximum (111)-contribution “Au(111)” was studied in 0.1 M pyridine + 0.05 M $HClO_4$ with SERS. No SERS signal could be detected on the untreated Au surface in the considered spectral range, as can be seen in Figure 8b. In contrast, the SERS spectrum of pyridine on the nanostructured electrode displays three bands. The two peaks at 1012 and 1039 cm^{-1} are associated with the ν_1 ring breathing mode and the ν_{12} symmetric

triangular ring deformation mode of pyridine, respectively. In addition, the third peak at 933 cm^{-1} is related to the presence of perchlorate (ClO_4^-) ions [59,60].

These observations indicate that these preferentially oriented electrodes can be used as substrates for SER spectroscopy and are supposed to be more advantageous compared to randomly roughened electrode surfaces for in-situ monitoring of electrochemical and electrocatalytic reactions.

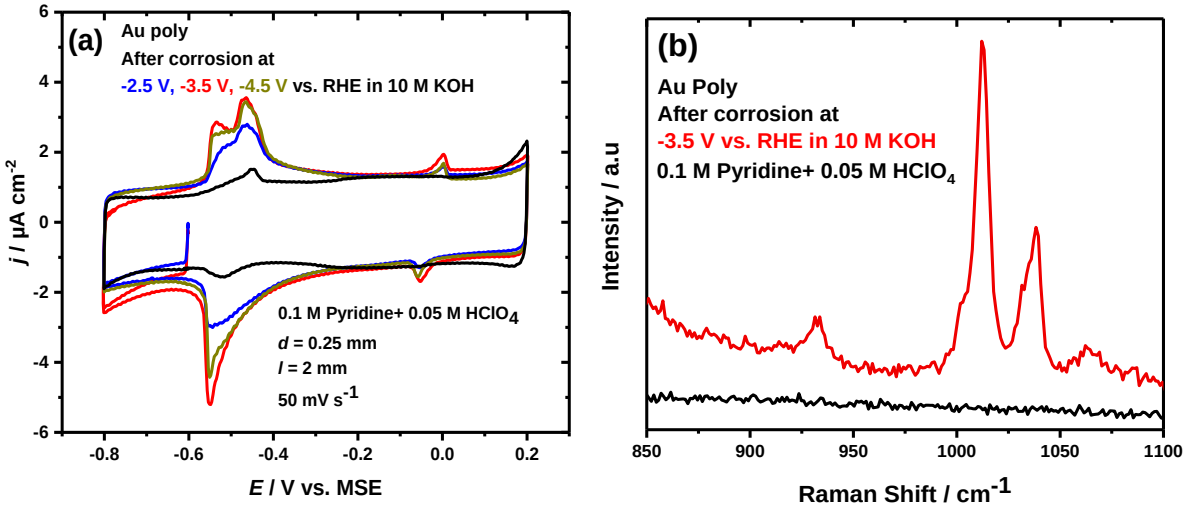

Figure 8: (a) Current-potential curves for polycrystalline gold in 0.05 M $HClO_4$ + 0.1 M pyridine at a scan rate of 50 mV s^{-1} before and after polarization in 10 M KOH at different voltages for 60 seconds (b) Raman spectra of polycrystalline gold in 0.05 M $HClO_4$ + 0.1 M pyridine before (black curve) and after (red curve) polarization in 10 M KOH at -3.5 V vs. RHE for 60 seconds. Spectra were obtained with a 633 nm laser at a power of 1.7 mW and an acquisition time of 20 s.

4. Conclusions

The stability of polycrystalline Au electrodes after polarization at negative potentials in highly concentrated KOH electrolytes (5-20 M) has been investigated. Cyclic voltamograms and SEM micrographs reveal that cathodic corrosion of Au wires can alert the facet distribution and enhance the electrochemically active surface area depending on the applied potential and on the KOH concentration. The hydrogen evolution seems to be a key element in the cathodic corrosion process. Furthermore, high near-surface concentration of K^+ is supposed to be crucial for cathodic corrosion because the highly negative potentials can only be achieved with appropriate counter-charges.

Structuring of polycrystalline Au electrodes in 10 M KOH at -3 V ≤ *E* ≤ -4 V vs. RHE leads to the generation of novel nanostructures with preferential (111)-texture and large EASA. The electrochemical measurements are complemented with SEM micrographs with respect to structural properties, such as EASA and crystallographic orientation.

The electrocatalytic activity of the nanostructured Au electrodes has been investigated towards the hydrogen evolution reaction (HER) and for the formic acid oxidation reaction (FAOR) in acidic media. The nanostructured Au electrodes with a high (111)-contribution behaves almost identically to an Au(111) single crystal towards FAOR. Furthermore, the combination of properties of Au(111) single crystals and Au nanoparticles shows enhanced HER activity, presumably due to the presence of highly-active low-coordination sites. The presence of low-coordination sites which is demonstrated by HER and supported by SEM do not seem to be very active for FAOR, despite their enhanced HER activity. In this way, the "Au(111)" surfaces can be used to identify electrocatalytically active enters.

In contrast to pristine Au wires and to well-ordered Au(111) single crystals, the nanostructured electrodes with preferential Au(111) facets show surface-enhanced Raman activity (SERS). These preferentially oriented electrodes can directly be used for SER spectroscopy for in-situ monitoring of electrochemical and electrocatalytic reactions.

Acknowledgments

References

1- F. Zaera, Probing Liquid/Solid Interfaces at the Molecular Level, Chem. Rev. 2012, 112, 2920–2986.

2- V. R. Stamenkovic, D. Strmcnik, P. P. Lopes, N. M. Markovic, Energy and fuels from electrochemical interfaces, Nat. Mater., 2017, 16, 57–69.

3- C. L. Bentley, M. Kang, P. R. Unwin, Nanoscale Surface Structure−Activity in Electrochemistry and Electrocatalysis, J. Am. Chem. Soc. 2019, 141, 2179−2193.

4- H.-G. Liao, Y.-X. Jiang, Z.-Y. Zhou, S.-P. Chen, S. G. Sun, Shape-Controlled Synthesis of Gold Nanoparticles in Deep Eutectic Solvents for Studies of Structure–Functionality Relationships in Electrocatalysis, Angew. Chem. Int. Ed. 2008, 47, 9100 –9103.

5- V. Climent, J. Feliu, Single Crystal Electrochemistry as an In-Situ Analytical Characterization Tool, Annu. Rev. Anal. Chem., 2020, 13, 22.1–22.22.

6- L. A. Kibler, Hydrogen Electrocatalysis, ChemPhysChem 2006, 7, 985 – 991.

7- S. Yoshimoto, K. Itaya, Adsorption and Assembly of Ions and Organic Molecules at Electrochemical Interfaces: Nanoscale Aspects, Annu. Rev. Anal. Chem. 2013, 6, 213–235.

8- A. Abdelrahman, J. M. Hermann, T. Jacob, L. A. Kibler, Adsorption of Acetate on Au(111): An in-situ Scanning Tunnelling Microscopy Study and Implications on Formic Acid Electrooxidation, ChemPhysChem 2019, 20, 2989–2996.

9- B. B. Blizanac, M. Arenz, P. N. Ross, N. M. Marković, Surface Electrochemistry of CO on Reconstructed Gold Single Crystal Surfaces Studied by Infrared Reflection Absorption Spectroscopy and Rotating Disk Electrode, J. Am. Chem. Soc. 2004, 126, 10130-10141.

10- T. Kondo, J. Morita, K. Hanaoka, S. Takakusagi, K. Tamura, M. Takahasi, J. Mizuki, K. Uosaki, Structure of Au(111) and Au(100) Single-Crystal Electrode Surfaces at Various Potentials in Sulfuric Acid Solution Determined by In Situ Surface X-ray Scattering, J. Phys. Chem. C 2007, 111, 13197-13204.

11- B. D. B. Aaronson, C.-H. Chen, H. Li, M. T. M. Koper, S. C. S. Lai, P. R. Unwin, Pseudo-Single-Crystal Electrochemistry on Polycrystalline Electrodes: Visualizing Activity at Grains and Grain Boundaries on Platinum for the Fe^{2+}/Fe^{3+} Redox Reaction, J. Am. Chem. Soc. 2013, 135, 3873−3880.

12- L. A. Kibler, M. Al-Shakran, Adsorption of Formate on Au(111) in Acid Solution: Relevance for Electro-Oxidation of Formic Acid, J. Phys. Chem. C 2016, 120, 16238−16245.

13- F. Bizzotto, H. Ouhbi, Y. Fu,G. K. H. Wiberg, U. Aschauer, M. Arenz, Examining the Structure Sensitivity of the Oxygen Evolution Reaction on Pt Single-Crystal Electrodes: A Combined Experimental and Theoretical Study, ChemPhysChem 2019, 20, 3154–3162.

14- A. T. Hubbard, Electrochemistry at well-characterized surfaces, Chem. Rev. 1988, 88, 633−656.

15- F. M. Schuett, D. Esau, K. L. Varvaris, S. Gelman, J. Björk, J. Rosen, G. Jerkiewicz, T. Jacob, Controlled-Atmosphere Flame Fusion Single-Crystal Growth of Non-Noble fcc, hcp, and bcc Metals Using Copper, Cobalt, and Iron, Angew. Chem. Int. Ed. 2020, 59,13246 –13252.

16- A. P. O'Mullane, From single crystal surfaces to single atoms: investigating active sites in electrocatalysis, Nanoscale, 2014, 6, 4012–4026.

17- F. J. V.-Iglesias, R. M. A.-Ais, J. S.-Gullón, E. Herrero, J. M. Feliu, Electrochemical Characterization of Shape-Controlled Pt Nanoparticles in Different Supporting Electrolytes, ACS Catal. 2012, 2, 901−910.

18- S. Neretina, R. A. Hughes, K. D. Gilroy, M. Hajfathalian, Noble Metal Nanostructure Synthesis at the Liquid−Substrate Interface: New Structures, New Insights, and New Possibilities, Acc. Chem. Res. 2016, 49, 2243−2250.

19- B. Hammer, J. K. Norskov, Why gold is the noblest of all the metals, Nature, 376, 1995, 238-240.

20- M. H. Dishner, M. M. Ivey, S. Gorer, J. C. Hemminger, F. J. Feher Preparation of gold thin films by epitaxial growth on mica and the effect of flame annealing, J. Vac. Sci. Technol. A 1998, 16, 3295.

21- N. Batina, T. Will, D. M. Kolb, Study of initial stages of copper deposition by in situ scanning tunneling microscopy, Faraday Discuss. 1992, 94, 93-106.

22- K. Uosaki, Y. Shen, T. Kondo, Preparation of a Highly Ordered Au (111) Phase on a Polycrystalline Gold Substrate by Vacuum Deposition and Its Characterization by XRD, GISXRD, STM/AFM, and Electrochemical Measurements, J. Phys. Chem. 1995, 99, 14117-14122.

23- M. R. Rahman, T. Okajima, T. Ohsaka, Fabrication of Au(111) nanoparticle-like electrode through a seed-mediated growth, Chem. Commun., 2010, 46, 5172–5174.

24- Y. Chen, S. Milenkovic, A. W. Hassel, {110}-Terminated Square-Shaped Gold Nanoplates and Their Electrochemical Surface Reactivity, ChemElectroChem 2017, 4, 557–564.

25- B. Seo, S. Choi, J. Kim, Simple Electrochemical Deposition of Au Nanoplates from Au(I) Cyanide Complexes and Their Electrocatalytic Activities, ACS Appl. Mater. Interfaces 2011, 3, 441–446.

26- A. Sukeri, M. Bertotti, Electrodeposited honeycomb-like dendritic porous gold surface: An efficient platform for enzyme-free hydrogen peroxide sensor at low overpotential, J. Electroanal. Chem. 2017, 805, 18–23.

27- D. Wang, P. Schaaf, Nanoporous gold nanoparticles. J. Mater. Chem., 2012, 22, 5344–5348.

28- C. L. Perdriel, A. J. Arvia, M. Ipohorski, Electrochemical Faceting of Polycrystalline Gold in 1 M H_2SO_4, J. Electroanal. Chem. Interfacial Electrochem. 1986, 215, 317–329.

29- P. Ahrens, M. Zander, U. Hasse, H. Wulff, C. Jeyabharathi, A. Kruth, F. Scholz, Electrochemical Formation of Gold Nanoparticles on Polycrystalline Gold Electrodes during Prolonged Potential Cycling, ChemElectroChem 2018, 5, 943–957.

30- A. Sukeri, L. Patricio, H. Saravia, M. Bertotti, A facile electrochemical approach to fabricate a nanoporous gold film electrode and its electrocatalytic activity towards dissolved oxygen reduction, Phys.Chem.Chem.Phys., 2015, 17, 28510-28514.

31- W. Huang, S. Chen, J. Zheng, Z. Li, Facile Preparation of Pt Hydrosols by Dispersing Bulk Pt with Potential Perturbations, Electrochem. Commun. 2009, 11, 469−472.

32- I. Leontyev, A. Kuriganova, Y. Kudryavtsev, B. Dkhil, N. Smirnova, New Life of a Forgotten Method: Electrochemical Route toward Highly Efficient Pt/C Catalysts for Low-Temperature Fuel Cells. Appl. Catal., A 2012, 431−432, 120−125.

33- F. Haber, The Phenomenon of the Formation of Metallic Dust from Cathodes. Trans. Am. Electrochem. Soc. 1902, 2, 189−196.

34- T. J. P. Hersbach, A. I. Yanson, M. T. M. Koper, Anisotropic etching of platinum electrodes at the onset of cathodic corrosion, Nat. Commun. 2016, 7, 12653.

35- T. J. P. Hersbach, I. T. McCrum, D. Anastasiadou, R. Wever, F. C.-Vallejo, M. T. M. Koper, Alkali Metal Cation Effects in Structuring Pt, Rh, and Au Surfaces through Cathodic Corrosion, ACS Appl. Mater. Interfaces, 2018,10, 39363-39379.

36- A. I. Yanson, P. Rodriguez, N. Garcia-Araez, R. V. Mom, F. D. Tichelaar, M. T. M. Koper, Cathodic Corrosion: A Quick, Clean, and Versatile Method for the Synthesis of Metallic Nanoparticles. Angew. Chem., Int. Ed. 2011, 50, 6346−6350.

37- J. N. Mills, I. T. McCrum, M. J. Janik, Alkali cation specific adsorption onto fcc(111) transition metal electrodes, Phys. Chem. Chem. Phys. 2014, 16, 13699.

38- T. J. P. Hersbach, V. A. Mints, F. C.-Vallejo, A. I. Yanson, M.T. M. Koper, Anisotropic etching of rhodium and gold as the onset of nanoparticle formation by cathodic corrosion, Faraday Discuss, 2016, 193, 207-222.

39- H. Ibach, Physics of Surfaces and Interfaces, 2006.

40- L. A. Kibler, Preparation and Characterization of Noble Metal Single Crystal Electrode Surfaces; ISE: Barcelona, 2003.

41- A. Hamelin, Cyclic voltammetry at gold single-crystal surfaces .1. Behaviour at low-index

42- L. A. Kibler, J. M. Hermann, A. Abdelrahman, A. A. El-Aziz, T. Jacob, New insights on hydrogen evolution at Au single crystal electrodes, Curr. Opin. in Electrochem. 2018, 9, 265–270.

43- C. Köntje, D. M. Kolb, G. Jerkiewicz, Roughening and Long-Range Nanopatterning of Au(111) through Potential Cycling in Aqueous Acidic Media, Langmuir, 2013, 29,10272−10278.

44- A. Speidel, R. Su, J. M.-Smith, P. Dryburgh, I. Bisterov, D. Pieris, W. Li, R. Patel, M. Clark, A. T. Clare, Crystallographic texture can be rapidly determined by electrochemical surface analytics, Acta Mater., 2018, 159, 89-101.

45- T. J.-Tonnies, I. Poltavsky, S. Ulrich, T. Moje, A. Tkatchenko, R. Herges, R. Berndt, Stability of functionalized platform molecules on Au(111), J. Chem. Phys. , 2018, 149, 244705.

46- H. Okamoto, T. B. Massalski, The Au−Cr (Gold-Chromium) system, Bull. Alloy Phase Diagrams 1985, 6, 224–228.

47- W. J. Hamer, Y. C. WU, Osmotic coefficients and mean activity coefficients of uni-univalent electrolytes in water at 25 °C, J. Phys. Chem. Ref. Data, 1972, 1, 1047−1100.

48- J. M. Hermann, A. Abdelrahman, T. Jacob, L. A. Kibler, Potential-dependent reconstruction kinetics probed by HER on Au(111) electrodes, Electrochim. Acta 2020, 347, 136287.

49- L. A. Kibler, M. Al-Shakran, Adsorption of Formate on Au(111) in Acid Solution: Relevance for Electro-Oxidation of Formic Acid, J. Phys. Chem. C 2016, 120, 16238−16245.

50- J. M. Hermann, Y. Mattausch, A. Weiß, T. Jacob, L. A. Kibler, Enhanced Electrocatalytic Oxidation of Formic Acid on Au(111) in the Presence of Pyridine, J. Electrochem. Soc. 2018, 165, J3192-J3198.

51- S. Brimaud, J. Solla-Gullón, I. Weber, J.M. Feliu, R.J. Behm, Formic acid electrooxidation on noble metal electrodes: The role of pH, surface structure and anion adsorption, and their mechanistic implication, ChemElectroChem 2014, 1, 1075 –1083.

52- J. Perez, E. R. Gonzalez, Hydrogen Evolution Reaction on Gold Single-Crystal Electrodes in Acid Solutions, J. Phys. Chem. B 1998, 102, 10931-10935.

53- T. D. Tran, M. T. T. Nguyen, H. V. Le, D. N. Nguyen, Q. Duc Truong, P. D. Tran, Gold nanoparticles as an outstanding catalyst for the hydrogen evolution reaction, Chem. Commun., 2018, 54, 3363—3366.

54- L. Stolberg, S. Morin, J. Lipkowski, D. E. Irish, Adsorption of pyridine at the Au(111)-solution interface, J. Electroanal. Chem. 1991, 307, 241-262.

55- J. F. Li, Y. J. Zhang, A. V. Rudnev, J. R. Anema, S. B. Li, W. J. Hong, P. Rajapandiyan, J. Lipowski, Z. Q. Tian, Electrochemical shell-isolated nanoparticle-enhanced Raman spectroscopy: correlating structural information and adsorption processes of pyridine at the Au(hkl) single crystal/solution interface, J. Am. Chem. Soc., 2015, 137, 2400-2408.

56- Z. Q. Tian, B. Ren, Adsorption and reaction at electrochemical interfaces as probed by surface-enhanced Raman spectroscopy, Annu. Rev. Phys. Chem. 2004, 55, 197.

57- J. F. Li, Y. F. Huang, Y. Ding, Z. L. Yang, S. B. Li, X. S. Zhou, F. R. Fan, W. Zhang, Z. Y. Zhou, D. Y. Wu, B. Ren, Z. L.Wang, Z. Q. Tian, Shell-isolated nanoparticle enhanced Raman spectroscopy, Nature 2010, 464, 392-396.

58- J. F. Li, Y. J. Zhang, A. V. Rudnev, J. R. Anema, S. B. Li, W. J. Hong, P. Rajapandiyan, J. Lipowski, Z. Q. Tian, Electrochemical shell-isolated nanoparticle-enhanced Raman

spectroscopy: correlating structural information and adsorption processes of pyridine at the Au(hkl) single crystal/solution interface, J. Am. Chem. Soc., 2015, 137, 2400-2408.

59- N. Ohta, I. Yagi, In Situ Surface-Enhanced Raman Scattering Spectroscopic Study of Pyridine Adsorbed on Gold Electrode Surfaces Comprised of Plasmonic Crystal Structures, J. Phys. Chem. C 2008, 112, 17603–17610.

60- B. Liu, A. Blaszczyk, M. Mayor, T. Wandlowski, Redox-Switching in a Viologen-Type Adlayer: An Electrochemical Shell-Isolated Nanoparticle Enhanced Raman Spectroscopy Study on Au(111)-(1x1) Single Crystal Electrodes. ACS Nano 2011, 5, 5662–5672.